Chin. Geogra. Sci. 2022 Vol. 32 No. 6 pp. 1110−1118
https://doi.org/10.1007/s11769-022-1285-1

Springer Science Press
www.springerlink.com/content/1002-0063

Spatial-temporal Characteristics of Holocene Paleosols in the Chinese Loess Plateau and Paleoclimatic Significance

GUO Xuelian[1], HE Lusheng[1], ZHAO Guoyong[2], WANG Weibin[1], CAO Huairen[1], WU Hao[1]

(1. *Key Laboratory of Western China's Mineral Resources of Gansu Province*, *School of Earth Sciences*, *Lanzhou University*, *Lanzhou* 730000, *China*; 2. *College of Urban and Environmental Science*, *Xinyang Normal University*, *Xinyang* 464000, *China*)

Abstract: The evolution of Holocene climate was investigated using grain size and magnetic susceptibility of the Holocene paleosols from Baicaoyuan (BCY), Xifeng (XF) and Linyou (LY) sections in the northwest, central and southern Chinese Loess Plateau (CLP). The results show that the Holocene in the BCY, XF and LY paleosol sections could be divided into three phases: during the early Holocene (11.8–10.5 kyr B. P.), increased magnetic susceptibility (χ) and frequency-dependent magnetic susceptibility (χ_{fd}) and decreased median grain size (Md) indicate that the East Asian Summer Monsoon (EASM) has become more intense and the climate has changed from cold to warm. During the middle Holocene (10.5–5.0 kyr B. P.), the values of χ, χ_{fd} and 2–5 μm grain-size fraction (GT2/5) are higher and Md and 30–63 μm grain-size fraction (GT30/63) are the lowest, which reflect a warm and humid regional climate. At ~ 8.0 kyr B. P., there was a transient dry-cold climatic spike corresponding to a Heinrich Event, the cold event was likely due to the collapse of the Laurentide ice sheet. During the late Holocene (5.0–0 kyr B. P.), χ and χ_{fd} values are the lowest, while Md and GT30/63 are high, as proxies of a weakened EASM, when the dry-cold climate prevailed in the region. Decreased irradiance since 5.0 kyr B.P. may have caused climatic cooling and drying. Spatially, the increased main peak values and skewness from BCY, XF to LY sections show that the grain size became fine, the East Asian Winter Monsoon (EAWM) reduced, and climate was warmer and wetter from northwest to southeast. In addition, Md can be used as alternative proxy for EAWM, while χ_{fd} is positive with the intensity of EASM under semiarid climate conditions in CLP.

Keywords: Holocene; magnetic susceptibility; grain size; paleoclimate; Chinese Loess Plateau (CLP)

Citation: GUO Xuelian, HE Lusheng, ZHAO Guoyong, WANG Weibin, CAO Huairen, WU Hao, 2022. Spatial-temporal Characteristics of Holocene Paleosols in the Chinese Loess Plateau and Paleoclimatic Significance. *Chinese Geographical Science*, 32(6): 1110−1118. https://doi.org/10.1007/s11769-022-1285-1

1 Introduction

The loess-paleosol sequences on the Chinese Loess Plateau (CLP) preserve abundant information of the paleoenvironment in the Asian interior and of the evolution of the East Asian Summer Monsoon (EASM) (An et al., 2001; Ding et al., 2002; Maher, 2016; Li et al., 2018).

The Holocene is the latest phase of global climate evolution, and Holocene paleoclimate history has been reconstructed by various archives including stalagmites (Wang et al., 2005; Verheyden et al., 2008; Kato et al., 2021), lake sediments (Dixit et al. 2014; Hamdan et al., 2020; Emmanouilidis et al., 2022), and eolian sedi-

Received date: 2021-12-30; accepted date: 2022-02-16
Foundation item: Under the auspices of the Second Tibetan Plateau Scientific Expedition and Research (STEP) program (No. 2019QZKK0704), Natural Science Foundation of China (No. 41772168, 42103046), Natural Science Foundation of Gansu Province (No. 20JR5RA272, 20JR5RA226)
Corresponding author: GUO Xuelian. E-mail: xlguo@lzu.edu.cn

ments (Senra et al., 2019; Li et al., 2022), with emphasis on the spatial and temporal variability of the EASM. The spatial variations of chemical weathering and paleoweathering in loess-paleosol sequences over the CLP from southeast to northwest are consistent with the modern rainfall gradient (Hao and Guo, 2005). However, the evolution of the EASM during the Holocene on the CLP remains controversial. The Holocene loess-paleosol sequences in the central of CLP show a distinct two-stage pattern of EASM, with a gradual increase during 13.1–8.5 kyr B. P. and a gradual decrease thereafter (Li et al., 2022). The EASM was strong and sandstorm activity was weak during 8500–6000 and 5000–3100 yr B.P. in the southern CLP (Zhao et al., 2020). While the middle Holocene is regarded as being warmer than the early and late Holocene (Wang et al., 2014; Senra et al., 2019), the Holocene megathermal episode was between 8.5–3.0 kyr B. P. (Shi et al., 1994). The optically stimulated luminescence (OSL) dating records in the Horqin desert in northern China suggest that the Holocene climatic optimum was from ~9 to 5 kyr B. P. (Guo et al., 2018a).

The EASM is characterized by alternating cold-dry and warm-wet climate cycles during the Holocene (An et al., 2015; Maher, 2016). The sediment grain-size and magnetic susceptibility (χ) are useful proxies for reconstructing the evolution of the East Asian winter monsoon (EAWM) (Ding et al., 2002; Stuut, 2007; Zhang et al., 2016) and the EASM (An et al., 2001; Orgeira et al., 2011; Maher, 2016; Zan et al., 2018; Jordanova and Jordanova, 2021). Previous studies of grain-size fractions demonstrated that > 30 μm grain-size fraction was sensitive to the EAWM in the central CLP, the > 40 μm grain-size fraction was a valid proxy in recording the EAWM in the western CLP (Wang et al., 2002), the median size was more sensitive to Holocene climate changes than susceptibility in the northern CLP (Zhao et al., 2013), < 2 μm fraction was a more accurate and sensitive indicator of weathering and soil formation in the western CLP (Guo et al., 2019), whereas the < 5 μm grain-size fraction was a robust indicator of pedogenic intensity and EASM under semiarid climatic conditions (Guo et al., 2011; Maher, 2016). Similarly, χ shows a positive correlation with pedogenic intensity in the central CLP and central Europe (Liu et al., 2001; Balsam et al., 2004; Jordanova and Jordanova, 2021). While it decreases with increased pedogenic intensity at the southern edge of the CLP (Han et al., 1996; Guo et al., 2018b). χ was mainly controlled by precipitation in soils (Guo et al., 2011). The χ and grain size parameters indicating the evolution of the East Asian monsoon are different in different regions of the CLP.

Although large numbers of researches had been conducted to study the variations of magnetic and grain-size parameters as the changes of temperature and/or precipitation, the patterns of various paleosols in different regions of the CLP has not yet been completely understood. Comparisons of the records among different climatic terms in the CLP with those distances of hundreds of kilometers obviously are beneficial to improve our understanding about this issue. This paper presents systematical magnetic susceptibility and grain size measurements of three Holocene paleosols from the sections of BCY in the northwestern CLP, XF in the central CLP and LY in the southern CLP to investigate changes of Holocene climate in different regions of the CLP. We analyzed grain size distributions and magnetic susceptibility characteristics for reliable proxies for the EAWM and EASM respectively, to explore the histories of Holocene climate at different climate setting.

2 Materials and Methods

The locations of the BCY, XF and LY sections are shown in Fig. 1. The BCY section (36°14′N, 105°08′E) is located at the northwest margin of the CLP, with a sub-frigid climate characterized by higher temperature and low precipitation in summer and dry-cold in winter. The annual mean temperature (MAT) is 6.5 °C, and the mean annual precipitation (MAP) is 366 mm (Zhao et al., 2013). The XF section (35°46′N, 107°41′E) is located in the central CLP and at the east of Liupan Mountains, with semi-arid climate by high temperature and precipitation in summer and dry-cold in winter. The MAT is 8.7 °C and the MAP is 550 mm (Guo et al., 2018b). The LY section (34°45′N, 107°49′E) is located in the southern CLP, northwest of Guanzhong Basin. The climate is semi-humid, with MAT of 9.1 °C and MAP of 680 mm (Guo et al., 2018b). The precipitations exhibit markedly decreasing trend from the southeast of the CLP to the northwest, which provide a good natural field for investigating the variations of relevant proxies.

Samples were taken at 2-cm interval for the BCY section and 5-cm interval for the XF and LY sections.

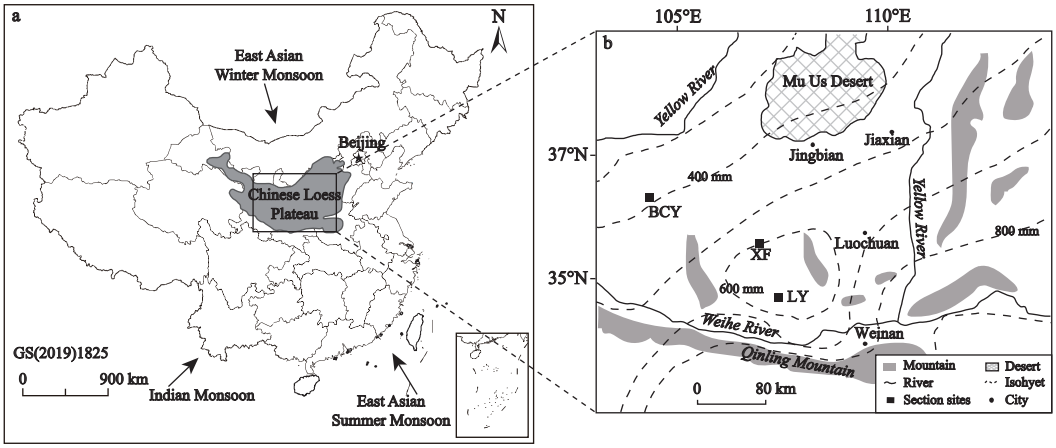

Fig. 1 The location of Chinese Loess Plateau with the wind directions of Indian monsoon and East Asian monsoons (Xue et al., 2016) (a), and the sites of Baicaoyuan (BCY), Xifeng (XF) and Linyou (LY) sections (b)

Ninety four samples for BCY, 29 samples for XF and 15 samples for LY profiles were obtained.

The magnetic susceptibility (χ) is typically used as a proxy of EASM intensity in the central of CLP and it reflects pedogenic intensity (Hao and Guo, 2005). The sample were air-dried at room temperature, weighed and packed in a nonmagnetic cubic plastic boxes of 8 ml volume. χ (mass-specific) was measured using Bartington Instruments MS-2 magnetic susceptibility meter (low frequency χ_{lf} with 470 Hz, high frequency χ_{hf} with 4700 Hz). The frequency-dependent magnetic susceptibility was calculated as follows: $\chi_{fd} = (\chi_{lf} - \chi_{hf})/\chi_{lf}$.

Grain size measurements have been widely applied to Chinese loess deposits for reconstructing variations in the intensity of the EAWM (Zhang et al., 2016). Grain-size distributions were measured using a British Malvern Mastersizer 2000 laser particle size analyzer with a measurement range of 0.02–2000 μm, with a 0.1Φ resolution and an absolute error of < 5% (Guo et al., 2019). All the measurements were completed in the Key Laboratory of West China's Environmental Systems, Ministry of Education, Lanzhou University.

3 Results

3.1 Grain sizes and magnetic susceptibility characteristics of BCY, XF and LY sections

The thickness of the Holocene paleosols of BCY, XF and LY sections are 1.88 m, 1.40 m and 0.70 m, respectively. Based on the research of BCY section (Zhao et al., 2013), comparing χ and grain size analyzed results of XF and LY sections with BCY section, we concluded that the Holocene in the BCY, XF and LY sections could be divided into three layers. The variations of grain size, χ and χ_{fd} curves of Holocene paleosols in BYC, XF and LY sections are shown in Fig. 2.

In BCY section (Fig. 2a), the values of Md (median grain size) and GT30/63 (30–63 μm grain-size fraction) are lower at depths of 1.88–1.76 m, where χ, χ_{fd} and GT2/5 (2–5 μm grain-size fraction) increase to the higher, which reflect a weaker EAWM and an increasing pedogenesis with enhanced EASM (Sun et al., 2004; Hao and Guo, 2005). The values of Md and GT30/63 are the lowest, and χ, χ_{fd} and GT2/5 arrive at the highest for depths of 1.76–0.60 m, indicating the weaker EAWM and the stronger pedogenesis degree. The values of χ, χ_{fd} and GT2/5 decline from 0.60–0 m, while the Md and GT30/63 increase, suggesting that the EAWM intensified and pedogenesis weakened. The χ_{fd} value is 6.6%–9.0%, means that superparamagnetic and coarse magnetic particles coexisting in samples (Dearing, 1999). These parameters show that the regional climate in the BCY changed from warm-state to more cold-state during the Holocene.

In XF section (Fig. 2b), the values of Md and GT30/63 are the lowest at depths of 1.40–1.20 m, while the χ, χ_{fd} and GT2/5 are the highest, which reflect the weak EAWM, and strong pedogenesis and EASM. From 1.20–0.92 m, the values of χ and χ_{fd} decrease, GT2/5 reduced rapidly to the lowest, while the Md and GT30/63 increased rapidly to the highest values, indicating that the EAWM intensified and the climate became dry and cold. From 0.92–0.35 m, the values of Md and GT30/63 are lower, but increase slightly, and χ, χ_{fd}

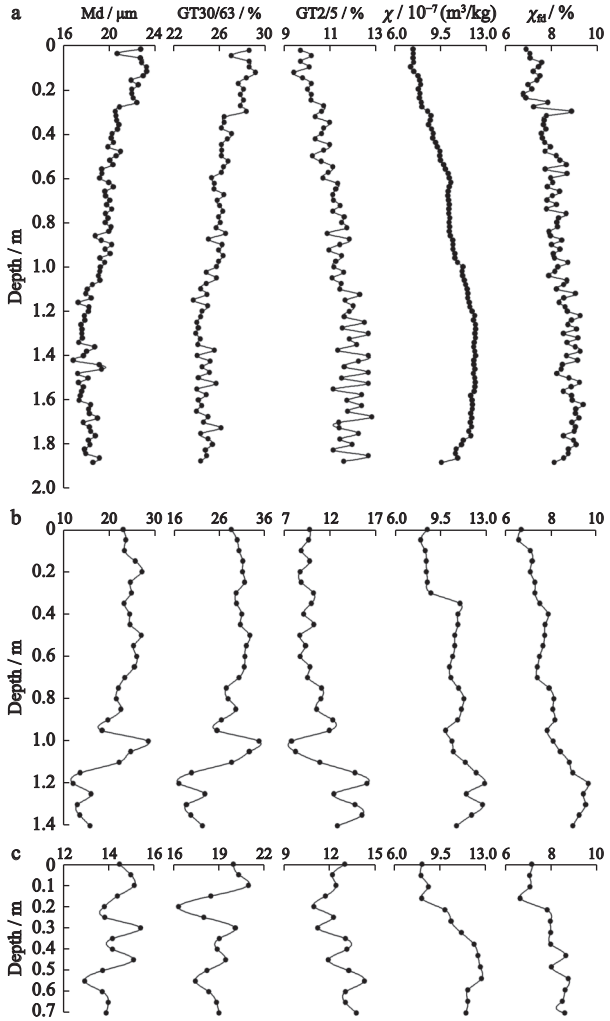

Fig. 2 Vertical distribution curves of grain size and magnetic susceptibility of Holocene paleosols in Baicaoyuan (a), Xifeng (b) and Linyou (c) sections. Md, median grain size; GT30/63, 30–63 μm grain-size fraction; GT2/5, 2–5 μm grain-size fraction; χ, magnetic susceptibility; χ_{fd}, frequency-dependent magnetic susceptibility

and GT2/5 are relatively higher, indicating a weaker EAWM with relatively warm-wet climate. From 0.35–0 m, the values of χ, χ_{fd} are the lowest, Md and GT30/63 are higher, indicating dry and cold climate. Overall, the decreasing trends of χ and χ_{fd} and increasing trends of Md and GT30/63 in XF section suggest that pedogenesis and EASM weakened, EAWM intensified. The climate became drier and colder during the Holocene.

In LY section (Fig. 2c), the values of Md and GT30/63 are low, χ and GT2/5 are high, χ_{fd} value is the highest at depth of 0.70–0.60 m, which may indicate strong EASM and weak EAWM, climate was warm-humid. Md and GT30/63 values have great fluctuation from 0.60–0.20 m, the values of χ, χ_{fd} and GT2/5 are the highest, indicating the strong pedogenesis and EASM. From 0.20–0 m, GT30/63 value rise steadily to the highest, the χ and χ_{fd} values are the lowest, indicating strong EAWM and weak pedogenesis, and the climate was dry and cold. Overall, the decreasing trends of χ, χ_{fd} in LY section indicate that the climate was colder and drier during the late Holocene.

3.2 The distribution characteristics of grain sizes in BCY, XF and LY sections

The grain size frequency distribution curves of paleosols from BCY, XF and LY sections are showed in Fig. 3. The frequency distribution curves of BCY section have an obvious main peak at 5.0 Φ and a sub-peak at 7.0 Φ (Fig. 3a), but the main peak are obvious at 5.5 Φ (Fig. 3b) and 6Φ (Fig. 3c), sub-peak at ~8.0 Φ are not obvious in XF and LY sections. The main peak values of BCY, XF and LY sections are 5 Φ, 5.5 Φ and 6.0 Φ, respectively, the mass percentage are 29%, 35% and 45%, respectively (Fig. 3), which show that the fine grains fraction increase from northwest to southeast in the CLP (Zhu, 2020). Similarly, skewness can reflect the size and sorting of grain size (Jiang, 2009). The skewness are 0.02, 0.27 and 0.29 from BCY, XF to LY, the increasing positive skewness reflects long tails of

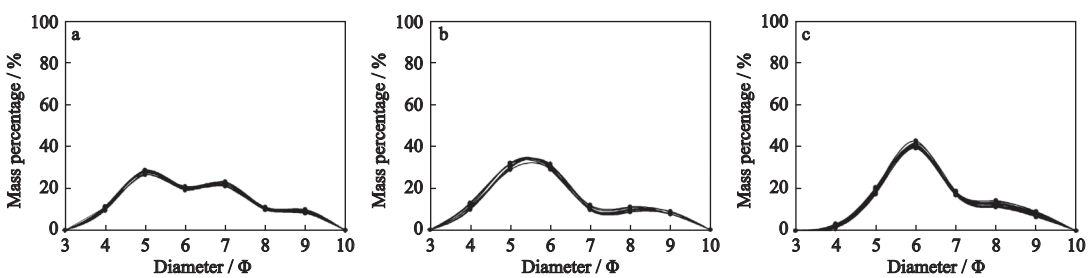

Fig. 3 Grain-size frequency distribution curves of paleosol samples from Baicaoyuan (a), Xifeng(b) and Linyou(c) sections on Chinese Loess Plateau

fine grain size. The main peak and skewness show that EAWM became weak from northwest to southeast in CLP during the Holocene.

4 Discussion

4.1 Chronological framework

Oxygen isotope records from stalagmites have the precision and resolution superior to loess-paleosol records, and the χ curves of three sections show similar trends with $\delta^{18}O$ variation in a stalagmite from Sanbao Cave (SB) (Fig. 4) (Wang et al., 2008). Comparing χ with the dated $\delta^{18}O$ of stalagmite from Sanbao Cave, we concluded the age of three phases in the Holocene (Fig. 4): 1) Early Holocene, the age of the lower boundary of early Holocene in three sections is ~11.8 kyr B. P., which is similar to the base of Holocene (11.7 kyr B. P.) defined by International Chronostratigraphic Chart (International Commission on Stratigraphy, 2018); 2) Middle Holocene, the age of the lower boundary of middle Holocene is ~10.5 kyr B. P.; (III) Late Holocene, the age of the lower boundary of late Holocene is ~5.0 kyr B. P.. The stalagmites from Xiniu Cave also recorded the middle Holocene about 10–5 kyr B. P. (Deng, 2017).

4.2 The climatic evolution during the Holocene

The evolution of Holocene climate in BCY, XF and LY regions are as follows: During the early Holocene (11.8–10.5 kyr B. P.), Md and GT30/63 in three sections declined, but χ and χ_{fd} values increased to a maximum (Fig. 2), reflecting a warmer climate after Younger Dryas event (Wang et al., 2008). During the middle Holocene (10.5–5.0 kyr B. P.), the Md and GT30/63 were low, but χ and χ_{fd} values were highest (Fig. 2), as evidence of an enhanced EASM and strong pedogenesis degree, this was the warmest and wettest period during the Holocene. During the late Holocene (5.0–0 kyr B. P.), χ and χ_{fd} values were the lowest, but Md and GT30/63 were high in three sections, which suggest that the EASM and pedogenesis weakened, the regional climate became dry and cold. The strengthening trend of EAWM during the late Holocene was caused by changes in middle- to high-latitude Northern Hemisphere atmospheric temperatures (Kang et al., 2020). Overall, the trends of Holocene climate evolution on CLP was consistent with the Holocene environmental changes in the Horqin desert in the northeastern China, which were controlled by movements of the EASM rainfall belt on a millennial time scale (Guo et al., 2018a).

Comparing the χ of BCY, XF and LY sections with the abundance of *Punctumorphana* in XF section and July solar insolation at latitude 65°N (Berger and Loutre, 1991), the variation trends are consistent (Fig. 5). The local climate change was related to July solar insolation: when the summer insolation gradient between middle and low latitudes increased, causing increased heat and vapor transportation from low latitude oceans to middle latitude continents, thus the EASM was intensified (Chen and Wu, 2008), the χ values and abundance of *Punctumorphana* increased during the early Holocene (Fig. 5), the climate was warmer and wetter. During the middle Holocene, the χ values were high and *Punctumorphana* thrived in this period, when the climate was the warmest and wettest (Chen and Wu, 2008). During the late Holocene, the χ values and abundance of *Punctumorphana* decreased with the declining July solar insolation gradient and cold and dry climate.

In conclusion, the climate of CLP rapidly warmed during the early Holocene (11.8–10.5 kyr B. P.), during the middle Holocene (10.5–5.0 kyr B. P.), it was the warmest and wettest period, but during the late Holocene (5.0–0 kyr B. P.), EAWM was intensified and the regional climate became dry and cold.

4.3 The spatial variation of Holocene climate in the CLP

The increased skewness and main peak values from BCY, XF to LY (Fig. 3) show that EAWM became weak and climate was warming from northwest to southeast in CLP during the Holocene. The grain size frequency distribution curves in BCY section has an obvious sub-peak at 7Φ, but the sub-peak at ~8Φ are not obvious in the XF and LY sections (Fig. 3). As the climate was warm, atmosphere pressure gradient decreased and EAWM was weak, and BCY belonged to monsoon area. EASM was resisted by the Liupan Mountains and winds could only carry fine grain size fractions (7Φ). When the climate was cold, it belonged to non-monsoon area and the strong EAWM carried coarse grains from northern deserts (Zhao et al., 2013). In contrast, XF and LY sections are located within the

monsoonal area. The grain kurtosis and skewness indicate that the grain sizes of BCY are finer than the sizes of XF and LY during the middle Holocene megathermal, which is consistent with the results of Md, GT30/63 and GT2/5 (Fig. 2).

The maximum values of χ and χ_{fd} increase from BCY (12.16 × $10^{-7}m^3$/kg, 8.88%) to XF (12.86 ×$10^{-7}m^3$/kg, 9.61%), then decrease in LY (12.68 ×$10^{-7}m^3$/kg, 8.73%) (Fig. 2). Modern mean annual precipitation increases from 366 mm, to 550 mm, and to 680 mm from BCY, XF to LY (Fig. 1), the EASM intensify. The BCY and XF sections are in the northwest edge and central CLP with well drained under semi-arid climate conditions, so there is a generally positive correlation between magnetic enhancement and pedogenesis (Ding et al., 1999; Balsam et al., 2004; Orgeira et al., 2011). However, LY has semi-humid climate, the moisture of the paleosol is higher and exceeds an upper threshold leading to transformation of the parts of fine ferrimagnetic minerals into weakly magnetic minerals, thus lowering magnetic susceptibility (Song et al., 2014; Guo et al., 2018b).

4.4 The climatic events at ~ 8.0 kyr B. P. and since 5.0 kyr B. P. in the East Asian summer monsoon area

XF section is located in the central CLP, east of Liupan Mountains, and showed rapidly decreased χ and χ_{fd} values at ~8.0 kyr B. P. (Fig. 4), as well as lower abundance of *Punctumorphana* snails (Fig. 2, 5), indicating cold and dry transient climatic events. The GT2/5, Md and GT30/63 curves of XF section also recorded the cold events at ~8.0 kyr B. P. (Fig. 2). Cold-dry climate at ~8.0 kyr B. P. corresponds to Heinrich event 5 in the North Atlantic Ocean (Bond et al., 1997). This event is also documented in lacustrine sediment (Dean et al., 2002; Dixit et al., 2014), stalagmites (Wang, 2008), and ice cores (Vinther et al., 2006; Thomas et al., 2007). There are two possible explanations for the weakening of the EASM at about 8.0 kyr B. P.. One explanation focuses on the collapse of the Laurentide ice sheet, which resulted in fresh water input and reduced thermohaline circulation in the North Atlantic Ocean. Diminished thermohaline circulation allows warm surface water to accumulate in the tropics and southern hemisphere, and this alters the heat balance between northern and southern hemisphere, resulting in a southward migration of the intertropical convergence zone as well as a weakening of the EASM (Wang et al., 2005; Fleitmann et al., 2008). Another explanation is that the Icelandic low pressure cell moved northeast due to the catastrophic melt-water event in the North Atlantic (Dean et al., 2002; Thomas et al., 2007).

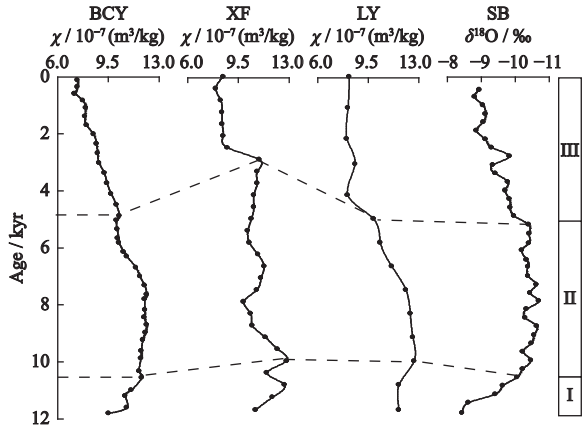

Fig. 4 A comparison diagram among magnetic susceptibility (χ) of Baicaoyuan (BCY), Xifeng (XF) and Linyou (LY) paleosols on Chinese Loess Plateau and $\delta^{18}O$ of stalagmites from Sanbao Cave (SB) (Wang et al., 2008)

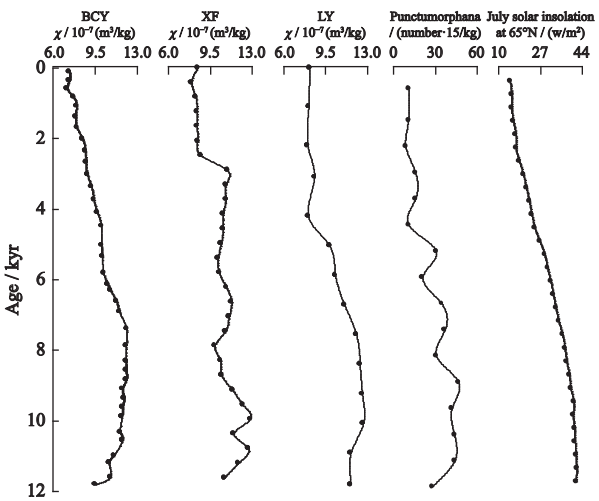

Fig. 5 The correlation between χ of Baicaoyuan (BCY), Xifeng (XF) and Linyou (LY) sections on Chinese Loess Plateau and the abundance of *Punctumorphana* in Xifeng section (Chen and Wu, 2008) and July Solar Insolation at 65°N (Berger and Loutre, 1991)

Weakening of EASM indicated by grain size and susceptibility since 5.0 kyr B. P. may be due to diminished thermal and pressure contrast between the continent and ocean as decrease of solar insolation (Fig. 5, Liu et al., 2009; Yan et al., 2015; Lan et al., 2020). Decreased monsoon moisture transport results in less precipitation in area controlled by the EASM. Records from peat

(Zhang et al., 2016; Sun et al., 2017), lacustrine sediment (Shen et al., 2005), stalagmites (Wang et al., 2008), desert sediment (Guo et al., 2018a), and the GRIP and NGRIP ice cores (Vinther et al., 2006) from northern hemisphere also reveal that the EASM weakened starting around 5.0 kyr B. P..

The mechanisms of the ~8.0 kyr B. P. and since 5.0 kyr B. P. cold events were different, the ~8.0 kyr B. P. cold event was likely due to the collapse of the Laurentide ice sheet, however, the decrease of irradiance since 5.0 kyr B. P. may has caused climatic cooling and drying since then.

5 Conclusions

The study show that Md has positive correlation with the intensity of EAWM in BCY, XF and LY sections, and it can be used as alternative proxy for the EAWM, while χ_{fd} has positive correlation with the intensity of EASM under semiarid climatic conditions in CLP.

The increased skewness and main peak values from BCY, XF to LY show that EAWM weaken and climate warming from northwest to southeast in CLP during the Holocene.

The χ_{fd} and χ values increased and coarse grain size fraction (Md) contents decreased from 11.8–10.5 kyr B. P., which indicate climate change from cold to warm after the Younger Dryas. During 10.5–5.0 kyr B. P., the higher values of χ_{fd} and χ reflect a warm-humid regional climate. At ~8.0 kyr B. P., a transient dry-cold climate corresponds to the North Atlantic Heinrich event 5. Since 5.0 kyr B. P., the χ values decreased and coarse grain fraction contents increased, which indicates the regional climate became dry and cold.

In summary, the climate was dry-cold at the beginning of the Holocene, then warm-wet during the middle Holocene, and it became drier and colder with the weakening EASM during the late Holocene.

References

An Z S, Kutzbach J E, Prell W L et al., 2001. Evolution of Asian monsoons and phased uplift of the Himalaya-Tibetan plateau since Late Miocene times. *Nature*, 411(6833): 62–66. doi: 10.1038/35075035

An Z S, Wu G X, Li J P et al., 2015. Global monsoon dynamics and climate change. *Annual Review of Earth and Planetary Sciences*, 43: 29–77. doi: 10.1146/annurev-earth-060313-054623

Balsam W, Ji J F, Chen J, 2004. Climatic interpretation of the Luochuan and Lingtai loess sections, China, based on changing iron oxide mineralogy and magnetic susceptibility. *Earth and Planetary Science Letters*, 223(3–4): 335–348. doi: 10.1016/j.epsl.2004.04.023

Berger A, Loutre M F, 1991. Insolation values for the climate of the last 10 million years. *Quaternary Science Reviews*, 10(4): 297–317. doi: 10.1016/0277-3791(91)90033-Q

Bond G, Showers W, Cheseby M et al., 1997. A pervasive millennial-scale cycle in North Atlantic Holocene and glacial climates. *Science*, 278(5341): 1257–1266. doi: 10.1126/science.278.5341.1257

Chen Xiaoyun, Wu Naiqin, 2008. Relatively warm-humid climate recorded by Mollusk species in the Chinese Loess Plateau during MIS3 and its possible forcing mechanism. *Quaternary Sciences*, 28(1): 154–161. (in Chinese)

Dean W E, Forester R M, Bardbury J P, 2002. Early Holocene change in atmospheric circulation in the Northern Great Plains: an upstream view of the 8.2 ka cold event. *Quaternary Science Reviews*, 21(16–17): 1763–1775. doi: 10.1016/S0277-3791(02)00002-1

Dearing J, 1999. Magnetic susceptibility. In: Walden J et al. (eds.). *Environmental Magnetism: A Practical Guide, Technical Guide*. London: Quaternary Research Association, 35–62.

Deng Shaolin, 2017. *Different Responses of Stalagmite Oxygen and Carbon Isotope Records to Holocene Climate*. Nanjing: Nanjing Normal University. (in Chinese)

Ding Z L, Xiong S F, Sun J M et al., 1999. Pedostratigraphy and paleomagnetism of a ~7.0 Ma eolian loess-red clay sequence at Lingtai, Loess Plateau, north-central China and the implications for paleomonsoon evolution. *Palaeogeography, Palaeoclimatology, Palaeoecology*, 152(1–2): 49–66. doi: 10.1016/S0031-0182(99)00034-6

Ding Z L, Derbyshire E, Yang S L et al., 2002. Stacked 2.6-Ma grain size record from the Chinese loess based on five sections and correlation with the deep-sea $\delta^{18}O$ record. *Paleoceanography*, 17(3): 5-1–5-21. doi: 10.1029/2001PA000725

Dixit Y, Hodell D A, Sinha R et al., 2014. Abrupt weakening of the Indian summer monsoon at 8.2 kyr B. P. *Earth and Planetary Science Letters*, 391: 16–23. doi: 10.1016/j.epsl.2014.01.026

Emmanouilidis A, Katrantsiotis C, Dotsika E et al., 2022. Holocene paleoclimate variability in the eastern Mediterranean, inferred from the multi-proxy record of Lake Vouliagmeni, Greece. *Palaeogeography, Palaeoclimatology, Palaeoecology*, 595: 110964. doi: 10.1016/j.palaeo.2022.110964

Fleitmann D, Mudelsee M, Burns S J et al., 2008. Evidence for a widespread climatic anomaly at around 9.2 ka before present. *Paleoceanography*, 23(1): PA1102. doi: 10.1029/2007pa001519

Guo B H, Peng T J, Feng Z T et al., 2019. Pedogenic components of Xijin loess from the western Chinese loess plateau with implications for the quaternary climate change. *Journal of Asi-*

an Earth Sciences, 170: 128–137. doi: 10.1016/j.jseaes.2018.11.012

Guo L C, Xiong S F, Yang P et al., 2018a. Holocene environmental changes in the Horqin desert revealed by OSL dating and $\delta^{13}C$ analyses of paleosols. *Quaternary International*, 469: 11–19. doi: 10.1016/j.quaint.2017.06.048

Guo Xuelian, Liu Xiuming, Lü Bin et al., 2011. Comparison of topsoil magnetic properties between the Loess Region in Tianshan Mountains and Loess Plateau, China, and its environmental significance. *Chinese Journal of Geophysics*, 54(4): 485–495. doi: 10.1002/cjg2.1631

Guo X L, Banerjee S K, Wang R H et al., 2018b. Why magnetite is not the only indicator of past rainfall in the Chinese Loess Plateau? *Geophysical Journal International*, 213(3): 2128–2137. doi: 10.1093/gji/ggy097

Hamdan M A, Flower R J, Hassan F A et al., 2020. Geochemical and palynological analysis of Faiyum Lake sediments, Egypt: implications for Holocene paleoclimate. *Journal of African earth sciences*, 167: 103864. doi: 10.1016/j.jafrearsci.2020.103864

Han J M, Lü H Y, Wu N Q et al., 1996. The magnetic susceptibility of modern soils in China and its use for paleoclimate reconstruction. *Studia Geophysica et Geodaetica*, 40(3): 262–275. doi: 10.1007/BF02300742

Hao Q Z, Guo Z T, 2005. Spatial variations of magnetic susceptibility of Chinese loess for the last 600 kyr: implications for monsoon evolution. *Journal of Geophysical Research:Solid Earth*, 110(B12): B12101. doi: 10.1029/2005JB003765

International Commission on Stratigraphy, 2018. International Chronostratigraphic Chart. *Journal of Stratigraphy*, 4: 365–370.

Jiang Mingli, 2009. Grain size analysis and its geological application. *Journal of Oil and Gas Technology*, 31(1): 161–163. (in Chinese)

Jordanova D, Jordanova N, 2021. Updating the significance and paleoclimate implications of magnetic susceptibility of Holocene loessic soils. *Geoderma*, 391: 114982. doi: 10.1016/j.geoderma.2021.114982

Kang S G, Du J H, Wang N et al., 2020. Early Holocene weakening and mid- to late Holocene strengthening of the East Asian winter monsoon. *Geology*, 48(11): 1043–1047. doi: 10.1130/G47621.1

Kato H, Amekawa S, Hori M et al., 2021. Influences of temperature and the meteoric water $\delta^{18}O$ value on a stalagmite record in the last deglacial to middle Holocene period from southwestern Japan. *Quaternary Science Reviews*, 253: 106746. doi: 10.1016/j.quascirev.2020.106746

Lan J H, Xu H, Lang Y C et al., 2020. Dramatic weakening of the East Asian summer monsoon in northern China during the transition from the Medieval Warm Period to the Little Ice Age. *Geology*, 48(4): 307–312. doi: 10.1130/G46811.1

Li P, Zhang C X, Wu H B et al., 2022. Geochemical characteristics of Holocene loess-paleosol sequences in central Chinese Loess Plateau and their implications for East Asian monsoon evolution. *Quaternary International*, 616: 99–108. doi: 10.1016/j.quaint.2021.10.017

Li Y R, Zhang W W, Aydin A et al., 2018. Formation of calcareous nodules in loess-paleosol sequences: reviews of existing models with a proposed new "per evapotranspiration model". *Journal of Asian Earth Sciences*, 154: 8–16. doi: 10.1016/j.jseaes.2017.12.002

Liu J, Wang B, Ding Q H et al., 2009. Centennial variations of the global monsoon precipitation in the last millennium: results from ECHO-G model. *Journal of Climate*, 22(9): 2356–2371. doi: 10.1175/2008JCLI2353.1

Liu Xiuming, An Zhisheng, Rolph T et al., 2001. Magnetic properties of the Tertiary red clay from Gansu. *Science in China Series D:Earth Sciences*, 44(7): 635–651. doi: 10.1007/BF02875337

Maher B A, 2016. Palaeoclimatic records of the loess/palaeosol sequences of the Chinese Loess Plateau. *Quaternary Science Reviews*, 154: 23–84. doi: 10.1016/j.quascirev.2016.08.004

Orgeira M J, Egli R, Compagnucci R H, 2011. A quantitative model of magnetic enhancement in Loessic soils. In: Petrovský E, Ivers D, Harinarayana T et al. (eds.). *The Earth's Magnetic Interior*. Dordrecht: Springer, 361 –397. doi: 10.1007/978-94-007-0323-0_25

Senra E O, Schaefer C E, Corrêa G R et al., 2019. Holocene pedogenesis along a chronotoposequence of soils from the Altiplano to the Cordillera Real, Bolivian Andes. *Catena*, 178: 141–153. doi: 10.1016/j.catena.2019.03.012

Shen J, Liu X Q, Wang S M et al., 2005. Palaeoclimatic changes in the Qinghai Lake area during the last 18, 000 years. *Quaternary International*, 136(1): 131–140. doi: 10.1016/j.quaint.2004.11.014

Shi Yafeng, Kong Zhaozheng, Wang Sumin et al., 1994. The climatic fluctuation and important events of Holocene megathermal in China. *Science in China (Series B)*, 37(3): 353–365. (in Chinese)

Song Y, Hao Q Z, Ge J Y et al. , 2014. Quantitative relationships between magnetic enhancement of modern soils and climatic variables over the Chinese Loess Plateau. *Quaternary International*, 334–335: 119–131. doi: 10.1016/j.quaint.2013.12.010

Stuut J, 2007. Grain-size records at ODP Site 1146 from the northern South China Sea: implications on the East Asian monsoon evolution since 20 Ma. *Science China Earth Sciences*, 10: 1536–1547.

Sun D H, Bloemendal J, Rea D K et al., 2004. Bimodal grain-size distribution of Chinese loess, and its palaeoclimatic implications. *Catena*, 55(3): 325–340. doi: 10.1016/S0341-8162(03)00109-7

Sun Xiaohong, Zhao Yan, Li Quan, 2017. Holocene peatland development and vegetation changes in the Zoige Basin, eastern Tibetan Plateau. *Science China Earth Sciences*, 60(10): 1826–1837. doi: 10.1007/s11430-017-9086-5

Thomas E R, Wolff E W, Mulvaney R et al., 2007. The 8.2 ka event from Greenland ice cores. *Quaternary Science Reviews*, 26(1–2): 70–81. doi: 10.1016/j.quascirev.2006.07.017

Verheyden S, Nader F H, Cheng H J et al., 2008. Paleoclimate reconstruction in the Levant region from the geochemistry of a Holocene stalagmite from the Jeita Cave, Lebanon. *Quaternary Research*, 70: 368–381. doi: 10.1016/j.yqres.2008.05.004

Vinther B M, Clausen H B, Johnsen S J et al., 2006. A synchronized dating of three Greenland ice cores throughout the Holocene. *Journal of Geophysical Research:Atmospheres*, 111(D13): D13102. doi: 10.1029/2005jd006921

Wang Haibin, Chen Fahu, Zhang Jiawu, 2002. Environmental significance of grain size of loess-paleosol sequence in western part of Chinese Loess Plateau. *Journal of Desert Research*, 22(1): 21–26. (in Chinese)

Wang H P, Chen J H, Zhang X J et al., 2014. Palaeosol development in the Chinese Loess Plateau as an indicator of the strength of the East Asian summer monsoon: evidence for a mid-Holocene maximum. *Quaternary International*, 334–335: 155–164. doi: 10.1016/j.quaint.2014.03.013

Wang Y J, Cheng H, Edwards R L et al., 2005. The Holocene Asian monsoon: links to solar changes and North Atlantic climate. *Science*, 308(5723): 854–857. doi: 10.1126/science.1106296

Wang Y J, Cheng H, Edwards R L et al., 2008. Millennial- and orbital-scale changes in the East Asian monsoon over the past 224, 000 years. *Nature*, 451(7182): 1090–1093. doi: 10.1038/nature06692

Xue J T, Dang X Y, Tang C Y et al., 2016. Fidelity of plant-wax molecular and carbon isotope ratios in a Holocene paleosol sequence from the Chinese Loess Plateau. *Organic Geochemistry*, 101: 176–183. doi: 10.1016/j.orggeochem.2016.09.004

Yan H, Wei W, Soon W et al., 2015. Dynamics of the intertropical convergence zone over the western Pacific during the Little Ice Age. *Nature Geoscience*, 8(4): 315–320. doi: 10.1038/NGEO2375

Zan J B, Fang X M, Zhang W L et al., 2018. A new record of late Pliocene-early Pleistocene aeolian loess-red clay deposits from the western Chinese Loess Plateau and its palaeoenvironmental implications. *Quaternary Science Reviews*, 186: 17–26. doi: 10.1016/j.quascirev.2018.02.010

Zhang W C, Yan H, Cheng P et al., 2016. Peatland development and climate changes in the Dajiuhu basin, central China, over the last 14, 100 years. *Quaternary International*, 425: 273–281. doi: 10.1016/j.quaint.2016.06.039

Zhao G Y, Liu X M, Chen Q et al., 2013. Paleoclimatic evolution of Holocene loess and discussion of the sensitivity of magnetic susceptibility and median diameter. *Quaternary International*, 296: 160–167. doi: 10.1016/j.quaint.2012.06.015

Zhao J B, Ma Y D, Cao J J et al., 2020. Holocene pedostratigraphic records from the southern Chinese Loess Plateau and their implications for the effects of climate on human civilization. *Catena*, 187: 104410. doi: 10.1016/j.catena.2019.104410

Zhu Xiaomin, 2020. *Sedimentary Petrology*. 5th ed. Beijing: Petroleum Industry Press. (in Chinese)